Porphyrin Functionalized Graphene Sheets in Aqueous Suspensions: From the Preparation of Graphene Sheets to Highly Conductive Graphene Films

ARTICLE *in* THE JOURNAL OF PHYSICAL CHEMISTRY C · APRIL 2010

Impact Factor: 4.77 · DOI: 10.1021/jp1008779

2 AUTHORS:

Jianxin Geng
Technical Institute of Physics and Chemistry
53 PUBLICATIONS **1,377** CITATIONS
SEE PROFILE

Hee-Tae Jung
Korea Advanced Institute of Science and Te…
153 PUBLICATIONS **2,796** CITATIONS
SEE PROFILE

Porphyrin Functionalized Graphene Sheets in Aqueous Suspensions: From the Preparation of Graphene Sheets to Highly Conductive Graphene Films

Jianxin Geng and Hee-Tae Jung*

National Research Laboratory, Department of Chemical and Biomolecular Engineering (BK-21), Korea Advanced Institute of Science and Technology, 373-1 Guseong-dong, Yuseong-gu, Daejeon 305-701, Korea

Received: January 29, 2010; Revised Manuscript Received: April 2, 2010

Graphene has a unique structure and potential applications in nanoelectronics, nanocomposites, conductive and transparent films, etc. Synthesis of graphene is one of the major research efforts in order to make rapid developments in graphene research. In this study, a new method, that makes use of the $\pi-\pi$ interactions between porphyrin and graphene to stabilize the chemically converted graphene (CCG), has been developed for preparation of CCG via chemical reduction of exfoliated graphene oxide (GO). Optical absorption spectroscopy measurement shows that $\pi-\pi$ interactions take place between GO and porphyrins, 5,10,15,20-tetraphenyl-21*H*, 23*H*-porphine-*p*,*p*′,*p*″,*p*‴-tetrasulfonic acid tetrasodium hydrate (TPP-SO_3Na) and 5,10,15,20-tetrakis(4-trimethylammoniophenyl) porphyrin tetra(*p*-toluenesulfonate). TPP-SO_3Na functionalized CCG can form a stable aqueous suspension due to the electrostatic repulsion between the CCG sheets, which results from the aggregation of TPP-SO_3Na molecules on the surfaces of the CCG sheets. Atomic force microscope observation shows that the TPP-SO_3Na functionalized CCG sheets are single-layer entities, which are sandwiched by TPP-SO_3Na molecules. Conductive graphene films with various thicknesses have been prepared by using the TPP-SO_3Na functionalized CCG suspension via a vacuum filtration method. It is found that the change of the sheet resistance of the CCG films follows the percolation mechanism. A sheet resistance as low as ca. 5 $K\Omega \cdot \square^{-1}$ of the CCG films with 80% transparency at 550 nm has been obtained. Such low sheet resistance is contributed to improved sp^2 networks of the CCG sheets, low contact resistance between the CCG sheets, and the healing of the defective vacancies on CCG sheets by porphyrin molecules, which are achieved by combination of chemical reduction of GO and thermal annealing of the resultant CCG films.

Introduction

Owing to the fact that graphene has many potentially important applications in the areas of field-effect transistors,[1] nanocomposites,[2] transparent and conductive films,[3−5] and molecular sensors,[6,7] to develop methods for preparing this material is a key goal of research efforts. Several procedures, including mechanical exfoliation,[8,9] dispersion of graphite in selective organic solvents,[10,11] chemical vapor deposition,[12−14] and the chemical method,[15] have been developed for this purpose. The chemical method, which is composed of acid oxidation of graphite powder and reduction of the exfoliated graphene oxide (GO), is superior in the preparation of single-layer graphene sheets and throughput to the others. However, reduction of GO in the absence of dispersants results in irreversible precipitation of the chemically converted graphene (CCG) as a result of its hydrophobic nature. Thus, it is essential to modify the GO surfaces and, consequently, the CCG surfaces, in order to enhance the dispersion of CCG sheets in a variety of solvents.

To date, three approaches for preparing dispersible CCG have been described. The first is chemical modification of the hydroxyl and carboxylic acid groups on the surfaces and edges of GO sheets by using phenyl isocyanate or alkylamine.[16−20] The chemically modified GO and, thereafter, the CCG can be stably dispersed in various organic solvents. These efforts lead to the applications of GO and the resultant CCG in graphene-based composites,[2] graphene-based electronics,[16] polymer solar cells,[17] and optical-limiting materials.[19] The second is selective reservation of the carboxylic groups at the edge areas of the GO sheets by performing the reduction at a basic condition, pH 10, so that when the interior of the GO sheets is reduced the negatively charged carboxylic groups can still provide enough electrostatic repulsion to stabilize the CCG in aqueous suspensions.[21] The third method is noncovalent functionalization of the CCG, which is based on the $\pi-\pi$ interactions of the CCG with conjugated polymers or aromatic molecules such as poly(sodium 4-styrenesulfonate), sulfonated polyaniline, 7,7,8,8-tetracyanoquinodimethane anion, and pyrene and perylenediimide decorated with water-soluble moieties.[22−26] In these cases, the sulfonated conjugated polymers and the decorated aromatic molecules function as anionic dispersants during the reduction of GO. The conjugated moieties provide strong affinity with the sp^2 domains of CCG sheets via π-stacking, while the anionic moieties provide electrostatic repulsion to stabilize the resulting functionalized CCG sheets in aqueous suspensions.

As an outstanding example of aromatic molecules, porphyrins have been widely studied for functionalization of carbon nanotubes (CNTs) on the basis of $\pi-\pi$ interactions between them: such interactions have been utilized in applications such as CNT separation, microstructure control of CNTs, and sunlight utilization.[27−30] Since both graphene and CNTs share the common feature of delocalized and conjugated electron structures, we expect that porphyrins would show similar interactions with graphene like those with CNTs. In the study described below, we have developed a new technique for producing dispersible CCG sheets in water. In this approach, water-soluble

* To whom correspondence should be addressed. E-mail: heetae@kaist.ac.kr. Phone: +82-42-350-3931. Fax: +82-42-350-8890.

10.1021/jp1008779
Published on Web 04/16/2010

porphyrins are used for noncovalent functionalization of the CCG sheets generated by hydrazine reduction of GO. We have found that the $\pi-\pi$ interactions taking place between porphyrins and graphene, as well as the porphyrin molecular architecture, play an important role in producing highly dispersible CCG sheets in water. In addition, the resulting porphyrin functionalized CCG sheets have been employed in the preparation of CCG films that have a low sheet resistance of ca. 5 $K\Omega\cdot\square^{-1}$ with 80% transparency at 550 nm.

Experimental Methods

Sample Preparation. GO was synthesized from graphite powder (Graphit Korpfmühl AG) by following a modified Hummers' method.[31−33] Briefly, $K_2S_2O_8$ (10 g) and P_2O_5 (10 g) were dissolved in concentrated H_2SO_4 (50 mL) at 80 °C. Graphite powder (12 g) was added to the acidic solution, and the resultant mixture was stirred at 80 °C for 4.5 h. After cooling to room temperature, the solution was diluted with deionized (DI) water (2 L), and allowed to stand overnight. The supernatant was decanted, and the pretreated graphite was obtained by vacuum filtration with a 0.2 μm PTFE membrane and washing with DI water (1 L). The precipitate was transferred to a Petri dish and dried in air for 1 d. To concentrated H_2SO_4 (460 mL) at <5 °C was added the pretreated graphite, followed by slow addition of $KMnO_4$ (60 g). Care was taken to keep the temperature of the solution below 10 °C. The mixture solution was then stirred at 35 °C for 2 h, cooled in an ice bath, and diluted with DI water (920 mL). The solution was further stirred for another 2 h, during which DI water (2.8 L) was added, followed by addition of a 30% H_2O_2 solution (50 mL). After the reaction mixture was kept standing overnight, the graphite oxide was obtained by centrifugation and subjected to cycles of suspension in 10% HCl solution and separation by centrifugation. A total of 5 L of 10% HCl solution was used, and the washing−separation cycle was repeated more than 20 times. In order to remove the free acid and remaining ions, the graphite oxide was subjected to cycles of washing with DI water and separation with centrifugation until the pH value of the supernatant reached 6. Finally, paper-like graphite oxide, which is dispersible in water and selective organic solvents,[34] was obtained after the precipitated slurry of graphite oxide was dried at 80 °C overnight in a vacuum oven.

A GO aqueous colloidal suspension was prepared by dispersing the paper-like graphite oxide in DI water with the aid of bath sonication. Reduction of GO was carried out by using hydrazine hydrate (50−60% aqueous solution) in a concentration ratio of GO:hydrazine = 1 mg:1 mmol in the presence of porphyrins (mass concentration ratio of GO:porphyrin = 1:4). In a control experiment, the GO was reduced in the absence of porphyrins. All reductions were carried out at 80 °C at the same time. The reactions were stopped when the CCG formed in the absence of porphyrins became fully flocculated (ca. 12 h).

Film Preparation. Graphene films were fabricated by using a vacuum filtration method.[35,36] A designated volume of a porphyrin functionalized CCG suspension (10 $mg\cdot L^{-1}$) was diluted with DI water (ca. 40 mL). The diluted suspension was subjected to vacuum filtration through an anodic aluminum oxide (AAO) membrane with a diameter of 25 mm and a pore size of 0.1 μm, leading to a CCG film deposited on the surface of the AAO membrane. After drying in a 60 °C oven, the AAO membrane was placed on the surface of a 3 M NaOH solution, leading to dissolution of the AAO membrane and depositing of the CCG film on the surface of the solution. The supporting solution was exchanged with a large volume of DI water, and then, the CCG film was transferred to the surface of a quartz or glass slide. Finally, the CCG film was dried in a 60 °C oven overnight. The thickness of the film was controlled by using different volumes of the CCG suspension. Thermal annealing of the CCG films was performed at 800 °C for 15 min in vacuum to further reduce the CCG. Pre-evacuation was required in order to protect the CCG films from thermal oxidation in the annealing process. Once the vacuum reached <60 mTorr, the CCG films were heated at a rate of 10 $°C\cdot min^{-1}$ when $T <$ 300 °C and at 20 $°C\cdot min^{-1}$ when 300 °C < T < 800 °C. After the temperature was held at 800 °C for 15 min, the annealing system was cooled down naturally.

Instrumentation. Zeta potentials of the aqueous suspensions of GO and GO/porphyrin composites were measured with a Zetasizer Nano ZS. The GO/porphyrin suspensions were prepared by mixing a designated volume of GO suspension (0.2 $mg\cdot mL^{-1}$) and porphyrin solution (0.1 $mg\cdot mL^{-1}$) to obtain a specific ratio of GO to porphyrin, followed by sonication for 10 min. Optical absorption spectra of the suspensions and transmittance spectra of films coated on quartz slides were recorded with a JASCO V-570 spectrophotometer. Steady-state photoluminescence (PL) spectra were obtained using a Shimadzu RF-5301 PC spectrofluorophotometer with an excitation wavelength of the maximum absorption in the optical absorption spectra. Raman spectroscopic analysis was carried out by using a high resolution dispersive Raman microscope (HORIBA Jobin Yvon HR800 UV) with an excitation laser of 514 nm. An ESCA 2000 X-ray photoelectron spectrometer (XPS) with a monochromated Mg Kα radiation of 1253.6 eV was used for elemental analyses of GO and CCG films. The film samples used for Raman and XPS measurement were prepared by the vacuum filtration method and deposited on glass surfaces. Atomic force microscope (AFM) images were obtained using a SPA 3800N microscope with a SPA-400 scanner. AFM samples were prepared by coating the GO and porphyrin functionalized CCG on newly cleaved mica surfaces. Thermal annealing of the CCG films was performed in a tube furnace (Barnstead 21100), equipped with a vacuum system. Electrical properties of CCG films were measured by coating two Au contacts on the top of the CCG films with the distance between the electrodes and the length of the electrodes being equal. $I-V$ curves of the devices made of CCG films were recorded using a Keithley 4200 Semiconductor Characterization System.

Results and Discussion

Interactions between GO and Porphyrins. Two different water-soluble porphyrins, 5,10,15,20-tetraphenyl-21*H*,23*H*-porphine-*p*,*p*′,*p*″,*p*‴-tetrasulfonic acid tetrasodium hydrate (TPP-SO_3Na) and 5,10,15,20-tetrakis(4-trimethylammoniophenyl) porphyrin tetra(*p*-toluenesulfonate) (TPP-ammonium), were employed in this study (Scheme 1). TPP-SO_3Na is negatively charged owing to the presence of sulfonate groups, whereas the quaternary ammonium groups in TPP-ammonium result in positive charges. The charges present in these substances can result in a combination of different types of interactions taking place between the porphyrins and GO, i.e., $\pi-\pi$ interactions and electrostatic repulsion between TPP-SO_3Na and GO and $\pi-\pi$ interactions and electrostatic attraction between TPP-ammonium and GO.

The $\pi-\pi$ interactions between GO and porphyrins, TPP-SO_3Na and TPP-ammonium, have been confirmed by using optical absorption and PL spectroscopy (Figure 1). In Figure 1a are displayed the optical absorption spectra of a series of GO/TPP-ammonium composite suspensions, in which TPP-

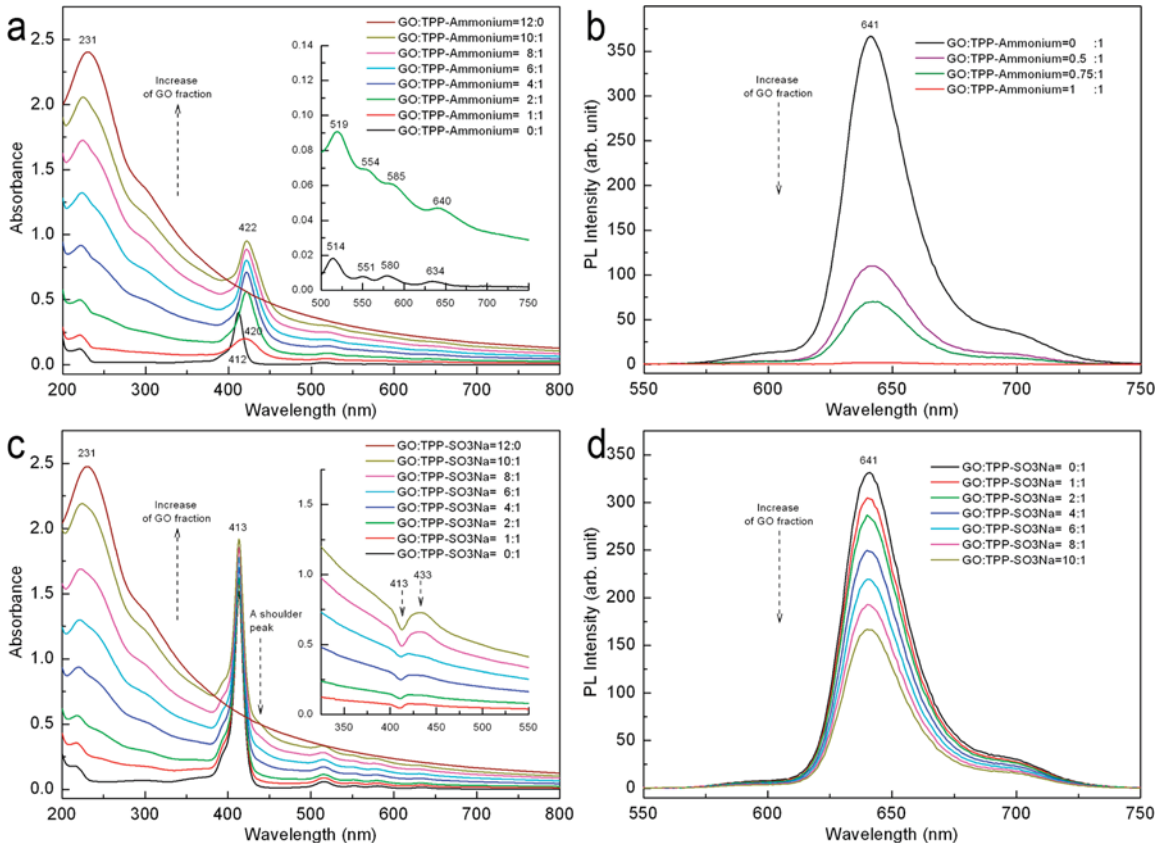

Figure 1. Optical absorption and PL spectra of GO/porphyrin aqueous suspensions: (a) optical absorption spectra and (b) PL spectra of GO/TPP-ammonium composite suspensions; (c) optical absorption spectra and (d) PL spectra of GO/TPP-SO_3Na composite suspensions.

SCHEME 1: Molecular Structures of TPP-SO_3Na and TPP-ammonium

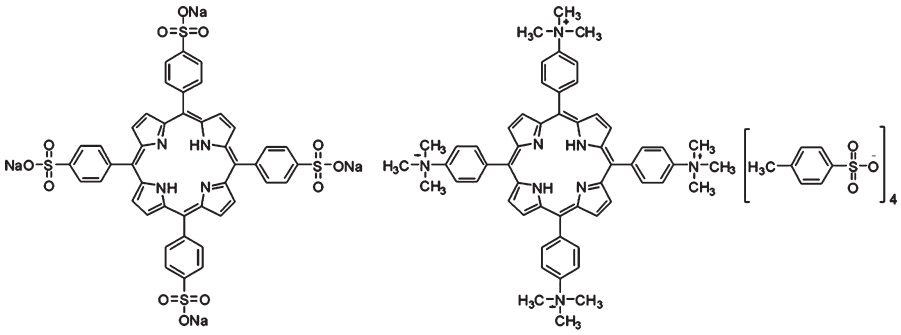

ammonium has a constant concentration of 0.005 mg·mL^{-1} and the concentration of GO is gradually increased. A GO suspension provides a characteristic absorption band at 231 nm (the purple line in Figure 1a). The spectrum of TPP-ammonium solution contains a strong peak at 412 nm attributed to the Soret band of porphyrin, as well as a group of weak peaks at 514, 551, 580, and 634 nm ascribed to the Q-bands of porphyrin (the black line in Figure 1a). Two spectral changes can be found upon mixing of GO and TPP-ammonium: the Soret band shifts from 412 to 422 nm; the TPP-ammonium Q-band peaks shift from 514, 551, 580, and 634 nm to 519, 554, 585, and 640 nm (the inset in Figure 1a). These findings indicate the $\pi-\pi$ interactions between GO and TPP-ammonium, which are in agreement with a previous report that the $\pi-\pi$ interactions between CCG and a pyrene derivative lead to a red shift of pyrene's feature absorption,[23] as well as a report that the interactions of a cationic porphyrin derivative with CCG result in a red shift of the porphyrin Soret band.[37] Note that the apparent blue shift of the absorption band of GO at 231 nm is due to the overlap with the band of porphyrin at ca. 220 nm. In Figure 1b is displayed the PL spectrum of TPP-ammonium along with the PL spectra of GO/TPP-ammonium composites with various ratios, excited with a wavelength of 420 nm. It is found that the PL of TPP-ammonium is quenched in the presence of GO, indicating that electron or energy transfer occurs from the excited state of TPP-ammonium to GO. This result is in agreement with the electron transfer from porphyrins to other carbon materials such as CNTs and fullerene.[38−40]

In Figure 1c and d are displayed the optical absorption and PL spectra of TPP-SO_3Na and the GO/TPP-SO_3Na composite suspensions. Compared to the spectrum of TPP-SO_3Na (the black line in Figure 1c), a shoulder peak is visible at ca. 433 nm on the right side of the TPP-SO_3Na Soret band in the spectra of GO/TPP-SO_3Na composites (Figure 1c), suggesting the $\pi-\pi$ interactions between GO and TPP-SO_3Na. This new shoulder peak has been confirmed by the GO/TPP-SO_3Na spectra

recorded through using a TPP-SO_3Na solution (with the same concentration as in the composite suspensions) as a reference (the inset of Figure 1c). A negative absorption peak at 413 nm, along with a broad positive absorption peak at 433 nm, is seen upon addition of GO into TPP-SO_3Na solution. The negative peak at 413 nm indicates that the concentration of free TPP-SO_3Na in the composite suspensions is lower than that in the TPP-SO_3Na reference solution, while the new positive absorption peak at 433 nm is due to TPP-SO_3Na J-aggregates, which arise from the $\pi-\pi$ interactions between TPP-SO_3Na and GO.[27,30] The $\pi-\pi$ interactions are short-range interactions so that the objects involved in these have to be very close to each other. However, electrostatic repulsion between TPP-SO_3Na and negatively charged GO may make it difficult for GO and TPP-SO_3Na to approach each other and reach the distance necessary to make $\pi-\pi$ interactions effective. Recently, other negatively charged π-conjugated water-soluble molecules were also reported to stabilize the CCG suspensions during the GO reduction,[22,23,25] although the $\pi-\pi$ interactions between them are not entirely understood. According to previous reports, it is likely that negatively charged carboxylic acid groups mainly situate on the edges of GO sheets so that the interior areas of GO sheets are relatively electrically neutral,[15,41] leaving possibilities for $\pi-\pi$ interactions to take place between the interior areas of GO sheets and TPP-SO_3Na. However, the spectral changes deriving from the $\pi-\pi$ interactions in the GO/TPP-SO_3Na system are not as marked as in the GO/TPP-ammonium system (Figure 1c vs 1a). The different extents of $\pi-\pi$ interactions in the GO/TPP-SO_3Na system and in the GO/TPP-ammonium system are also confirmed by the PL quenching effect. In Figure 1d are displayed the PL spectra of TPP-SO_3Na and GO/TPP-SO_3Na composites, excited with a wavelength of 413 nm. It is found that GO shows a much lower quenching efficiency in the GO/TPP-SO_3Na system than in the GO/TPP-ammonium system. For example, the PL of TPP-ammonium can be entirely quenched by GO in a 1:1 GO/TPP-ammonium composite (the red line in Figure 1b); however, the quenching efficiency of GO at this component ratio in the GO/TPP-SO_3Na composite is much lower (the red line in Figure 1d). Thus, a conclusion can be drawn that the more dramatic spectral changes of TPP-ammonium and the higher quenching efficiency of GO in the GO/TPP-ammonium system (Figure 1a,b) than in the GO/TPP-SO_3Na system (Figure 1c,d) are the consequence of enhanced $\pi-\pi$ interactions between GO sheets and TPP-ammonium due to the electrostatic attraction between them, whereas the electrostatic repulsion in the GO/TPP-SO_3Na system weakens the $\pi-\pi$ interactions.

Although both TPP-SO_3Na and TPP-ammonium are found to interact with GO based on π-stacking, they lead to different phenomena upon addition into a GO suspension. The observation made in this investigation shows that the negatively charged TPP-SO_3Na enhances the dispersibility of GO in water. Addition of TPP-SO_3Na to a GO suspension results in the formation of a more stable GO/TPP-SO_3Na composite suspension. In contrast, the GO/TPP-ammonium suspension can only be stable temporally, with precipitate observed during the storage of a GO/TPP-ammonium suspension (the inset in Figure 2). The effect of TPP-SO_3Na is a consequence of the increased negative charges on the composite surfaces, which promote electrostatic repulsion between GO sheets, because of the aggregation of TPP-SO_3Na molecules on the surfaces of GO sheets due to the $\pi-\pi$ interactions between them. The charge alterations that result from attachment of TPP-SO_3Na and TPP-ammonium to the GO surfaces were probed by measuring the zeta potential

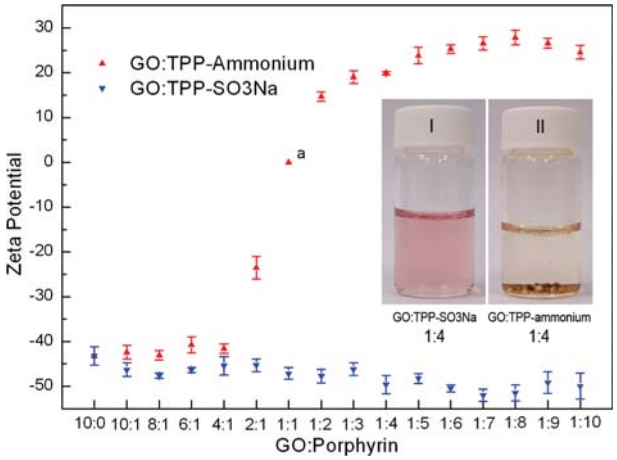

Figure 2. Changes of the zeta potential of the GO/porphyrin composite suspensions as a function of the component ratio. In the 1:1 GO/porphyrin composite suspension, both components have a concentration of 0.005 mg·mL^{-1}. In the suspensions on the left side of the 1:1 GO/porphyrin composite, the content of GO is increased and the porphyrin concentration is held constant, while, on the right side of the 1:1 ratio, the porphyrin content is increased and the GO concentration is held constant. The error bars in the graph show the standard deviation of the sample, which is obtained on the basis of the data of five measurements for each suspension. The potential value of point a is arbitrarily set at 0 because the charge density on CCG sheets for this suspension is too low to obtain an experimental value in measurement. The inset shows GO suspensions mixed with (I) TPP-SO_3Na and (II) TPP-ammonium.

of the composite suspensions (Figure 2). An aqueous suspension of GO exhibits a zeta potential of ca. −43, indicative of negatively charged surfaces caused by the presence of hydrophilic carboxylic acid groups.[21] As the TPP-SO_3Na content is increased in GO/TPP-SO_3Na composites, the zeta potential of the composite suspensions becomes more negative (ca. −50) due to the aggregation of negatively charged TPP-SO_3Na on the GO surfaces. The small changes of the zeta potential of GO suspensions upon addition of TPP-SO_3Na are in agreement with the weak $\pi-\pi$ interactions between GO and TPP-SO_3Na (Figure 1c). In contrast, the zeta potential of GO/TPP-ammonium composite suspensions changes from ca. −43 to ca. +28 as the TPP-ammonium content is increased in the composites. In this case, the negative charges on the surfaces of GO sheets are canceled by the positively charged quaternary ammonium groups. The fact that TPP-ammonium molecules can continue aggregating on GO surfaces after the zeta potential of the GO/TPP-ammonium composite suspension turns to a positive value demonstrates the existence of $\pi-\pi$ interactions between GO and TPP-ammonium.

Reduction of GO to CCG. Reduction of GO was carried out by using hydrazine hydrate. Visual inspection (the inset in Figure 3b) of the product shows that a homogeneous CCG suspension is obtained when GO is reduced in the presence of TPP-SO_3Na (bottle I, GO = 0.02 mg·mL^{-1} and a weight component ratio of GO:TPP-SO_3Na = 1:4). However, the CCG forms a precipitate when reduction is performed in the absence of TPP-SO_3Na (bottle II) and in the presence of TPP-ammonium (bottle III). These findings indicate that the TPP-SO_3Na is effective in bringing about dispersal of CCG sheets in water due to the negatively charged CCG surfaces that result from the attachment of TPP-SO_3Na molecules on the CCG surfaces. Zeta potential measurement shows that a TPP-SO_3Na functionalized CCG suspension has a potential of ca. −61 so that this suspension is stable and no precipitate is found even after it

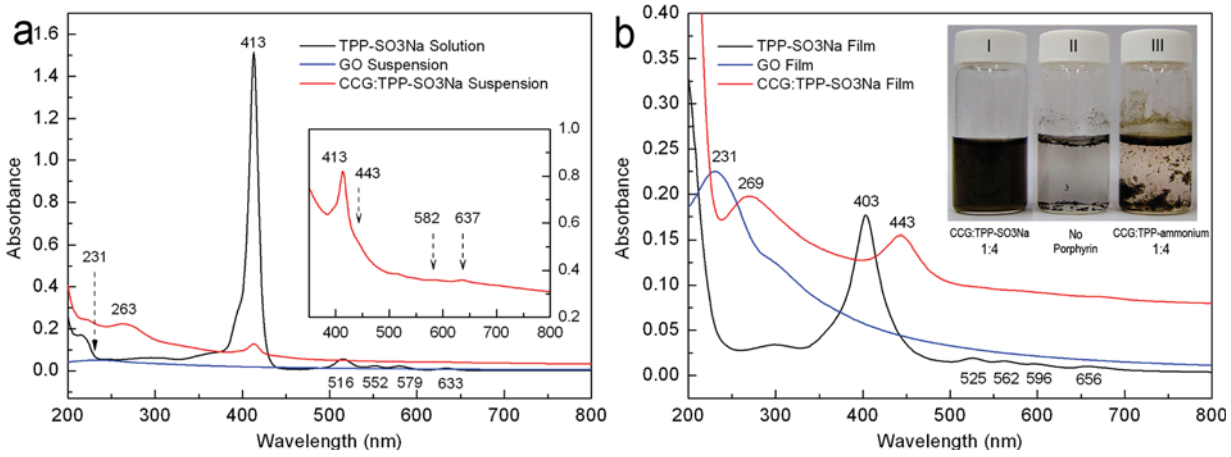

Figure 3. UV−visible spectra of (a) a TPP-SO_3Na solution, a GO suspension, a CCG/TPP-SO_3Na suspension, and a highly concentrated CCG/TPP-SO_3Na suspension (CCG = 0.02 mg·ml^{-1}) in the inset and (b) a TPP-SO_3Na film prepared on a quartz surface by casting a TPP-SO_3Na solution, and GO and TPP-SO_3Na functionalized CCG films prepared on quartz surfaces by the vacuum filtration method. In the inset of Figure 3b are displayed the pictures of CCG suspensions in the presence of TPP-SO_3Na (I), in the absence of porphyrin (II), and in the presence of TPP-ammonium (III).

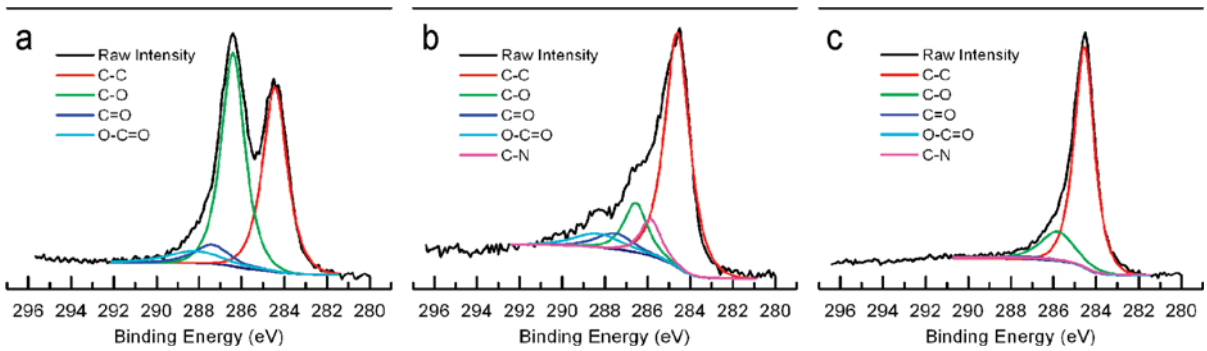

Figure 4. C 1s XPS spectra of (a) GO, (b) TPP-SO_3Na functionalized CCG, and (c) thermally annealed CCG film.

has been kept standing for several months. The conversion of GO to CCG in the presence of TPP-SO_3Na was confirmed by using XPS. In Figure 4a is shown the C 1s XPS spectrum of GO, which contains two dominant peaks at 284.5 and 286.4 eV corresponding to C−C and C−O species, along with two weak peaks at 287.5 and 288.2 eV corresponding to C═O and O−C═O species.[34,42] The peaks at 286.4, 287.5, and 288.2 eV indicate the presence of hydroxyl, epoxy, carbonyl, and carboxylic acid groups on the surfaces and edges of GO sheets. Upon reduction of GO (Figure 4b), the intensity of the peaks corresponding to O−C═O, C═O, and especially C−O species are reduced, indicative of the removal of the oxygen containing groups, which is accompanied by recovery of the sp^2 carbon networks. Meanwhile, a new peak corresponding to C−N species, which result from the bond formation by hydrazine, appears at 285.7 eV in the spectra of CCG (Figure 4b).[24,26] In Figure 4c is shown the XPS of thermally annealed CCG, which contains the peaks corresponding to C−C and C−O species only, indicating that the CCG has been further reduced during the thermal annealing. Additionally, compared to the spectrum of nonannealed CCG, the intensity of the O 1s peak relative to the C 1s peak is much reduced, with no N 1s peak detected, in the XPS survey of the thermal annealed CCG (not shown).

The $\pi-\pi$ interactions taking place between CCG and TPP-SO_3Na were identified by using UV−visible spectroscopy (Figure 3). In Figure 3a are displayed the spectra of a TPP-SO_3Na solution (0.005 mg·mL^{-1}), a GO suspension (0.00125 mg·mL^{-1}), and a CCG/TPP-SO_3Na composite suspension (CCG:TPP-SO_3Na = 1:4, TPP-SO_3Na = 0.005 mg·mL^{-1}). The spectrum of the TPP-SO_3Na solution shows characteristic absorption peaks at 413 nm ascribed to the TPP-SO_3Na Soret band, and at 516, 552, 579, and 633 nm corresponding to the Q-bands of TPP-SO_3Na.[27] The GO suspension yields a spectrum containing a feature absorption band at 231 nm. However, the CCG/TPP-SO_3Na suspension yields a spectrum containing markedly reduced characteristic absorption peaks of TPP-SO_3Na, with increased absorption in the whole UV−visible range, and an absorption peak at 263 nm contributed to CCG. Apparently, the marked reduction of TPP-SO_3Na characteristic absorption peaks in the CCG/TPP-SO_3Na spectrum is contributed to the interactions between CCG and TPP-SO_3Na. Compared to the spectrum of the GO suspension, the overall increased absorption of the CCG/TPP-SO_3Na suspension is ascribed to the chemical conversion of GO to CCG. In the inset of Figure 3a is displayed a magnified spectrum of the CCG/TPP-SO_3Na suspension. It is found that a shoulder peak appears at ca. 443 nm, and that two Q-band peaks are accurately discerned at 582 and 637 nm, which show red shifts compared to the corresponding peaks in the TPP-SO_3Na spectrum. These findings clearly show the existence of the $\pi-\pi$ interactions between CCG and TPP-SO_3Na. In Figure 3b are displayed the UV−visible spectra of TPP-SO_3Na, GO, and CCG/TPP-SO_3Na composite in the solid state. The spectrum of a TPP-SO_3Na film contains a strong absorption band at 403 nm attributable to the porphyrin Soret band, as well as a group of weak peaks at 525, 562, 596, and 656 nm ascribed to the Q-bands of the porphyrin chromophore.[27] The spectrum of a GO film contains a characteristic absorption band at 231 nm.[21] However, the film of TPP-SO_3Na functionalized CCG exhibits

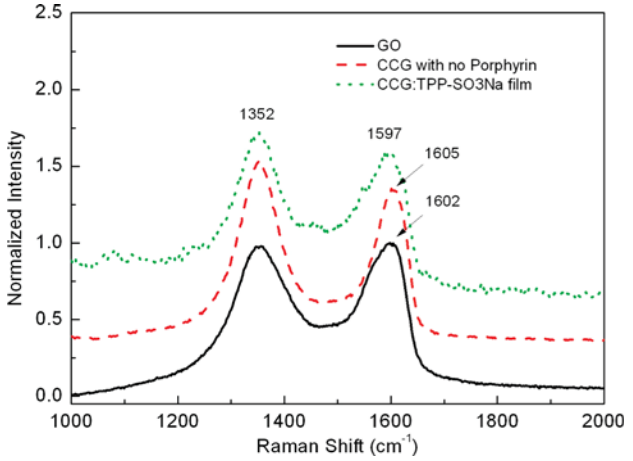

Figure 5. Raman spectra of GO, CCG, and TPP-SO_3Na functionalized CCG. The specimen CCG with no porphyrin was prepared by drop-casting the CCG precipitate obtained in the absence of porphyrin on a glass surface. The GO and CCG/TPP-SO_3Na films were prepared on glass surfaces via the vacuum filtration method. The spectra were normalized by the G-band intensity.

a spectrum that contains peaks at 269 nm, corresponding to the characteristic absorption band of CCG, and at 443 nm ascribed to porphyrin J-aggregates, which is in agreement with the fact that CNTs induce the formation of porphyrin J-aggregates also.[27,30] In this case, the Q-bands are not detected. The CCG/TPP-SO_3Na composite shows a more significant absorption band of porphyrin J-aggregates in the solid state than in aqueous suspensions because CCG and TPP-SO_3Na are closer to each other in the solid state. These results indicate that hydrazine promoted conversion of GO to CCG has taken place and that $\pi-\pi$ interactions exist between CCG and TPP-SO_3Na in a manner similar to that seen between CNTs and porphyrins.[27−30] The shift observed in the Soret band is also in agreement with the report that $\pi-\pi$ interactions between graphene and pyrene or porphyrin derivatives lead to a red shift of the characteristic absorption of pyrene or porphyrin.[23,37]

The interactions between the CCG and TPP-SO_3Na, as well as the structural changes occurring during the conversion of GO to CCG, were also characterized by using Raman spectroscopy (Figure 5). The Raman spectrum of GO (the black solid line) shows two broad peaks at 1352 and 1602 cm^{-1}, which correspond to the D- and G-bands of graphene. After GO is chemically converted to CCG (the red dashed line), the D- and G-band peaks become narrower and the G-band shifts to 1605 cm^{-1}, with an increase in the D/G intensity ratio compared to that observed in GO. The increase of the D/G intensity ratio suggests that the average size of the sp^2 domains is decreased upon reduction of the GO sheets.[43] In contrast, the CCG obtained in the presence of TPP-SO_3Na shows broadened D- and G-band peaks (the green dotted line), with the G-band peak shifted to 1597 cm^{-1} compared to the CCG obtained in the absence of porphyrin (the red dashed line). The shift of the G-band is contributed to electron doping that is a consequence of the $\pi-\pi$ interactions between TPP-SO_3Na and CCG sheets.[44,45]

The morphology and thickness of individual GO and TPP-SO_3Na functionalized CCG sheets have been studied by AFM observation. In Figure 6a is displayed an image of GO sheets with lateral dimensions ranging from submicrometer to several micrometers and a thickness of ca. 1 nm. The thickness of the sheets is greater than the theoretical value (0.34 nm) owing to the presence of functional groups on the sheet surfaces.[22,43,46] It is noteworthy that the contrast of the images at the edges of

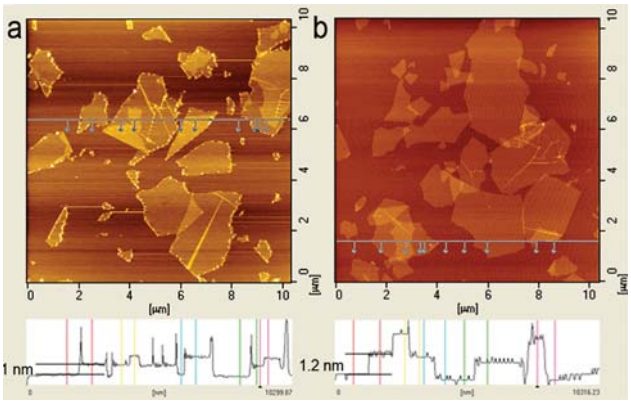

Figure 6. AFM images of (a) GO sheets and (b) TPP-SO_3Na functionalized CCG sheets.

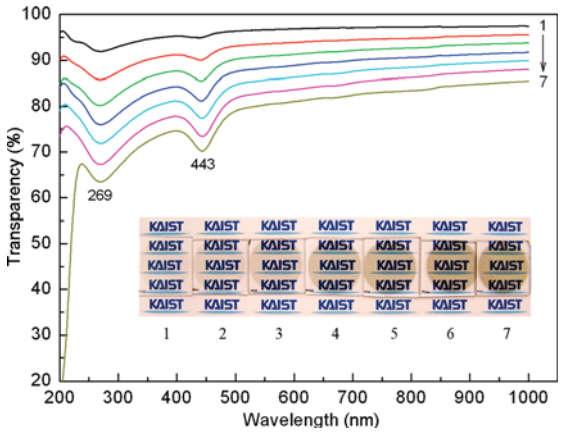

Figure 7. Transmittance spectra of CCG films prepared with various volumes of a 10 mg·L^{-1} TPP-SO_3Na functionalized CCG suspension: 80, 160, 240, 320, 400, 480, and 560 μL for the spectra numbered from 1 to 7. The inset shows visual transparency of these CCG films.

the GO sheets is higher than that of interior regions. This phenomenon is likely caused by the presence of a higher density of functional groups on the edges. In Figure 6b is shown an image of TPP-SO_3Na functionalized CCG sheets. No high contrast regions are observed on the edges of the CCG sheets, since the functional groups are removed during reduction of GO. Cross-section analysis shows that the thickness of the TPP-SO_3Na functionalized CCG sheets is slightly increased to ca. 1.2 nm as a consequence of the attachment of porphyrin layers on one or two sides of the CCG sheets.[22,23]

Optical and Electrical Properties of CCG Films. To demonstrate the superiority of this approach to forming dispersible CCG sheets in water, we prepared graphene films of various thicknesses by using the vacuum filtration method.[35,36] The thicknesses of the films are controlled by varying the volume of the suspension employed for film preparation. In Figure 7 are shown the transmittance spectra of the CCG films generated by using 80, 160, 240, 320, 400, 480, and 560 μL of a 10 mg·L^{-1} TPP-SO_3Na functionalized CCG suspension, respectively. The transparency of the CCG films is decreased as the suspension volume used for film preparation is increased. Each of the spectra contains two absorption peaks at 269 and 443 nm, which correspond to the characteristic absorption bands of CCG and TPP-SO_3Na J-aggregates. The contrast of the word "KAIST" beneath the CCG films coated on quartz slides indicates the film transparency visually (the inset in Figure 7).

In Figure 8 are displayed the plots of the transparency (Figure 8a) of the CCG films at 550 nm as a function of the volume of

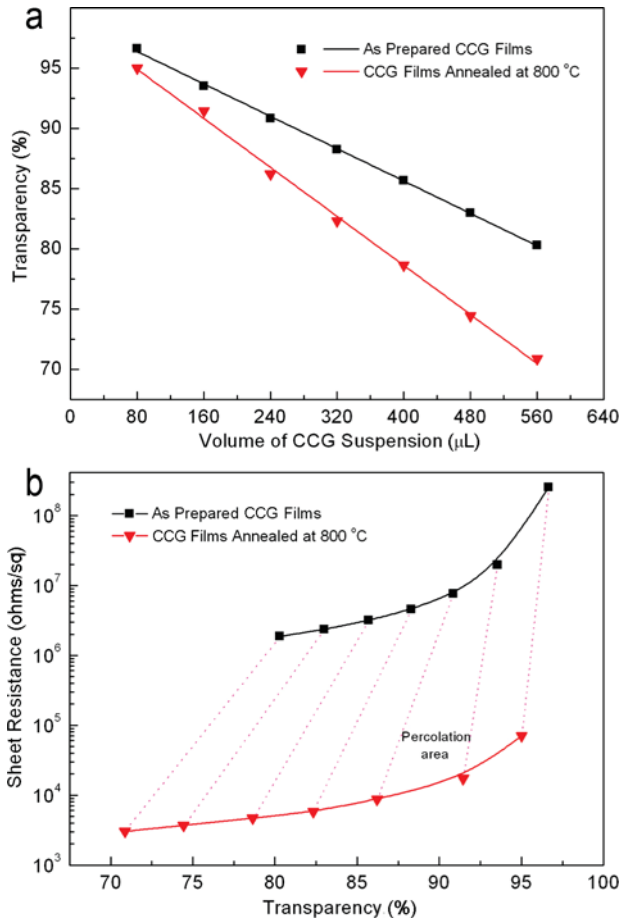

Figure 8. Optical and electrical properties of CCG films: (a) the change of transparency of the CCG films at 550 nm as a function of the volume (μL) of the 10 mg·L^{-1} TPP-SO_3Na functionalized CCG suspension used for film preparation; (b) the change of sheet resistance of the CCG films as a function of the film transparency. The dotted lines link the sheet resistances of each CCG film before and after thermal annealing.

the CCG suspension used for film preparation and the plots of sheet resistance (Figure 8b) of the CCG films as a function of the film transparency. It is found that the transparency of the CCG films decreases linearly with increasing suspension volume (the black square line in Figure 8a), indicating that the film thickness can be accurately controlled by changing the suspension volume. In addition, the sheet resistance of the CCG films is decreased as the film transparency is reduced, with an inflection point that locates between the films prepared with 160 and 240 μL suspensions (the black square line in Figure 8b). This inflection point corresponds to the percolation of the CCG sheets in the films.[35] Furthermore, we have observed that thermal annealing of the films affects both the transparency and the sheet resistance of the CCG films. The transparency becomes several percent lower after the CCG films are thermally annealed at 800 °C (the red triangle line in Figure 8a), whereas the sheet resistance experiences a 3 orders of magnitude decrease (the red triangle line in Figure 8b). The decrease of transparency of the CCG films upon thermal annealing can be explained by thermal improvement of the sp^2 domains, which is confirmed by XPS (Figure 4c). The thermally annealed CCG film yields a XPS spectrum that contains markedly reduced peaks corresponding to the C—O, C═O, O—C═O, and C—N species, indicative of the thermal reduction of CCG and improved sp^2 networks in the resultant CCG sheets.[3,47] It is well-known that both chemical reduction and thermal annealing of GO sheets result in recovery of the sp^2 domains,[3,47] which is accompanied by increased absorption in the whole UV−visible range. In Figure 3 is shown that a CCG solution or film yields enhanced absorption compared to a GO solution or film. Therefore, a conclusion can be drawn that the decreased transparency of the CCG films upon thermal annealing is contributed to thermally improved sp^2 domains in the CCG sheets. As for the electrical property, the decrease of the sheet resistance of the CCG films upon thermal annealing reflects the structural changes that include an enhancement of the contacts between the CCG sheets and an improvement of the sp^2 domains of the CCG sheets (Figure 4c). In addition, the porphyrin molecules attached on the CCG surfaces may heal the defective vacancies on the CCG sheets during thermal annealing due to the fact that nanographene molecules are likely to be cross-linked to construct graphene sheets by thermal treatment.[5] As a result, the sheet resistance of the CCG films after thermal annealing reaches as low as ca. 5 K$\Omega\cdot\square^{-1}$ with 80% transparency at 550 nm. Among the transparent and conductive CCG films reported, most of them have been made by hydrazine vapor reduction of GO films.[3,4,47,48] The sheet resistance of the film reaches saturation when the film becomes thicker because the vapor reduction is only effective for the uppermost layer.[3] In our case, the GO sheets are reduced in aqueous suspensions. Our CCG films have a bulk conductivity of ca. 370 $\Omega\cdot$cm^{-1} with a transparency of 80% at 550 nm, which is one of the highest conductivity values for the CCG films thermally annealed at similar conditions (800 °C).[3,5,47−49] This is due to the maximum restoration of the sp^2 domains that is achieved by a combination of chemical reduction in aqueous suspension and thermal reduction of the CCG films.[26] The key point of this paper is to develop a new method for preparing highly dispersible CCG in aqueous suspensions through porphyrin noncovalent functionalization, which does not interfere with the restoration of the sp^2 domains during chemical reduction, and even provide possibilities to heal the defective vacancies in CCG sheets during thermal annealing.[5]

Conclusions

The investigation described above has led to a new method for the preparation of dispersible graphene sheets that involves the use of hydrazine reduction of GO in the presence of the porphyrin derivative TPP-SO_3Na as a dispersant. The negatively charged porphyrin promotes generation of highly dispersed CCG sheets in water as a consequence of both its aggregation to the CCG sheets driven by $\pi-\pi$ interactions and its effect of bringing a number of negative charges on the CCG surfaces. The sheet resistance of the CCG films produced in this manner is as low as ca. 5 K$\Omega\cdot\square^{-1}$ with 80% transparency at 550 nm, which is achieved by guaranteeing the maximum recovery of the sp^2 networks by a combination of chemical and thermal reductions. We expect that the observations made in this effort will stimulate new studies of graphene in application such as transparent electrodes, microelectronics, and photosensitized composite devices.

Acknowledgment. This work was supported by the National Research Laboratory Program of the Korea Science and Engineering Foundation (KOSEF), the World Class University Program (R32-2008-000-10142-0), and the Center for Nanoscale Mechatronics & Manufacturing (08K140100414, CNMM).

References and Notes

(1) Sui, Y.; Appenzeller, J. Screening and Interlayer Coupling in Multilayer Graphene Field-Effect Transistors. *Nano Lett.* **2009**, *9*, 2973–2977.

(2) Stankovich, S.; Dikin, D. A.; Dommett, G. H. B.; Kohlhaas, K. M.; Zimney, E. J.; Stach, E. A.; Piner, R. D.; Nguyen, S. T.; Ruoff, R. S. Graphene-based composite materials. *Nature* **2006**, *442*, 282–286.

(3) Eda, G.; Fanchini, G.; Chhowalla, M. Large-area ultrathin films of reduced graphene oxide as a transparent and flexible electronic material. *Nat. Nanotechnol.* **2008**, *3*, 270–274.

(4) Becerril, H. A.; Mao, J.; Liu, Z.; Stoltenberg, R. M.; Bao, Z.; Chen, Y. Evaluation of Solution-Processed Reduced Graphene Oxide Films as Transparent Conductors. *ACS Nano* **2008**, *2*, 463–470.

(5) Wang, X.; Zhi, L.; Tsao, N.; Tomović, Z.; Li, J.; Mullen, K. Transparent Carbon Films as Electrodes in Organic Solar Cells. *Angew. Chem., Int. Ed.* **2008**, *47*, 2990–2992.

(6) Schedin, F.; Geim, A. K.; Morozov, S. V.; Hill, E. W.; Blake, P.; Katsnelson, M. I.; Novoselov, K. S. Detection of individual gas molecules adsorbed on graphene. *Nat. Mater.* **2007**, *6*, 652–655.

(7) Lu, C. H.; Yang, H. H.; Zhu, C. L.; Chen, X.; Chen, G. N. A Graphene Platform for Sensing Biomolecules. *Angew. Chem., Int. Ed.* **2009**, *48*, 4785–4787.

(8) Novoselov, K. S.; Geim, A. K.; Morozov, S. V.; Jiang, D.; Zhang, Y.; Dubonos, S. V.; Grigorieva, I. V.; Firsov, A. A. Electric Field Effect in Atomically Thin Carbon Films. *Science* **2004**, *306*, 666–669.

(9) Liang, X.; Chang, A. S. P.; Zhang, Y.; Harteneck, B. D.; Choo, H.; Olynick, D. L.; Cabrini, S. Electrostatic Force Assisted Exfoliation of Prepatterned Few-Layer Graphenes into Device Sites. *Nano Lett.* **2009**, *9*, 467–472.

(10) Hernandez, Y.; Nicolosi, V.; Lotya, M.; Blighe, F. M.; Sun, Z. Y.; De, S.; McGovern, I. T.; Holland, B.; Byrne, M.; Gun'ko, Y. K.; Boland, J. J.; Niraj, P.; Duesberg, G.; Krishnamurthy, S.; Goodhue, R.; Hutchison, J.; Scardaci, V.; Ferrari, A. C.; Coleman, J. N. High-yield production of graphene by liquid-phase exfoliation of graphite. *Nat. Nanotechnol.* **2008**, *3*, 563–568.

(11) Biswas, S.; Drzal, L. T. A Novel Approach to Create a Highly Ordered Monolayer Film of Graphene Nanosheets at the Liquid-Liquid Interface. *Nano Lett.* **2009**, *9*, 167–172.

(12) Kim, K. S.; Zhao, Y.; Jang, H.; Lee, S. Y.; Kim, J. M.; Kim, K. S.; Ahn, J.-H.; Kim, P.; Choi, J.-Y.; Hong, B. H. Large-scale pattern growth of graphene films for stretchable transparent electrodes. *Nature* **2009**, *457*, 706–710.

(13) Berger, C.; Song, Z. M.; Li, X. B.; Wu, X. S.; Brown, N.; Naud, C.; Mayou, D.; Li, T. B.; Hass, J.; Marchenkov, A. N.; Conrad, E. H.; First, P. N.; de Heer, W. A. Electronic confinement and coherence in patterned epitaxial graphene. *Science* **2006**, *312*, 1191–1196.

(14) Reina, A.; Jia, X.; Ho, J.; Nezich, D.; Son, H.; Bulovic, V.; Dresselhaus, M. S.; Kong, J. Large Area, Few-Layer Graphene Films on Arbitrary Substrates by Chemical Vapor Deposition. *Nano Lett.* **2009**, *9*, 30–35.

(15) Park, S.; Ruoff, R. S. Chemical methods for the production of graphenes. *Nat. Nanotechnol.* **2009**, *4*, 217–224.

(16) Eda, G.; Chhowalla, M. Graphene-based Composite Thin Films for Electronics. *Nano Lett.* **2009**, *9*, 814–818.

(17) Liu, Z.; Liu, Q.; Huang, Y.; Ma, Y.; Yin, S.; Zhang, X.; Sun, W.; Chen, Y. Organic Photovoltaic Devices Based on a Novel Acceptor Material: Graphene. *Adv. Mater.* **2008**, *20*, 3924–3930.

(18) Stankovich, S.; Piner, R. D.; Nguyen, S. T.; Ruoff, R. S. Synthesis and exfoliation of isocyanate-treated graphene oxide nanoplatelets. *Carbon* **2006**, *44*, 3342–3347.

(19) Xu, Y.; Liu, Z.; Zhang, X.; Wang, Y.; Tian, J.; Huang, Y.; Ma, Y.; Zhang, X.; Chen, Y. A Graphene Hybrid Material Covalently Functionalized with Porphyrin: Synthesis and Optical Limiting Property. *Adv. Mater.* **2009**, *21*, 1275–1279.

(20) Niyogi, S.; Bekyarova, E.; Itkis, M. E.; McWilliams, J. L.; Hamon, M. A.; Haddon, R. C. Solution Properties of Graphite and Graphene. *J. Am. Chem. Soc.* **2006**, *128*, 7720–7721.

(21) Li, D.; Muller, M. B.; Gilje, S.; Kaner, R. B.; Wallace, G. G. Processable aqueous dispersions of graphene nanosheets. *Nat. Nanotechnol.* **2008**, *3*, 101–105.

(22) Stankovich, S.; Piner, R. D.; Chen, X.; Wu, N.; Nguyen, S. T.; Ruoff, R. S. Stable aqueous dispersions of graphitic nanoplatelets via the reduction of exfoliated graphite oxide in the presence of poly(sodium 4-styrenesulfonate). *J. Mater. Chem.* **2006**, *16*, 155–158.

(23) Xu, Y.; Bai, H.; Lu, G.; Li, C.; Shi, G. Flexible Graphene Films via the Filtration of Water-Soluble Noncovalent Functionalized Graphene Sheets. *J. Am. Chem. Soc.* **2008**, *130*, 5856–5857.

(24) Bai, H.; Xu, Y.; Zhao, L.; Li, C.; Shi, G. Non-covalent functionalization of graphene sheets by sulfonated polyaniline. *Chem. Commun.* **2009**, 1667–1669.

(25) Hao, R.; Qian, W.; Zhang, L.; Hou, Y. Aqueous dispersions of TCNQ-anion-stabilized graphene sheets. *Chem. Commun.* **2008**, 6576–6578.

(26) Su, Q.; Pang, S.; Alijani, V.; Li, C.; Feng, X.; Müllen, K. Composites of Graphene with Large Aromatic Molecules. *Adv. Mater.* **2009**, *21*, 3191–3195.

(27) Geng, J. X.; Ko, Y. K.; Youn, S. C.; Kim, Y. H.; Kim, S. A.; Jung, D. H.; Jung, H. T. Synthesis of SWNT rings by noncovalent hybridization of porphyrins and single-walled carbon nanotubes. *J. Phys. Chem. C* **2008**, *112*, 12264–12271.

(28) Li, H. P.; Zhou, B.; Lin, Y.; Gu, L. R.; Wang, W.; Fernando, K. A. S.; Kumar, S.; Allard, L. F.; Sun, Y. P. Selective interactions of porphyrins with semiconducting single-walled carbon nanotubes. *J. Am. Chem. Soc.* **2004**, *126*, 1014–1015.

(29) Hasobe, T.; Fukuzumi, S.; Kamat, P. V. Organized assemblies of single wall carbon nanotubes and porphyrin for photochemical solar cells: Charge injection from excited porphyrin into single-walled carbon nanotubes. *J. Phys. Chem. B* **2006**, *110*, 25477–25484.

(30) Hasobe, T.; Fukuzumi, S.; Kamat, P. V. Ordered assembly of protonated porphyrin driven by single-wall carbon nanotubes. J- and H-aggregates to nanorods. *J. Am. Chem. Soc.* **2005**, *127*, 11884–11885.

(31) Gilje, S.; Han, S.; Wang, M.; Wang, K. L.; Kaner, R. B. A chemical route to graphene for device applications. *Nano Lett.* **2007**, *7*, 3394–3398.

(32) Hummers, W. S.; Offeman, R. E. Preparation of Graphitic Oxide. *J. Am. Chem. Soc.* **1958**, *80*, 1339–1339.

(33) Kovtyukhova, N. I.; Ollivier, P. J.; Martin, B. R.; Mallouk, T. E.; Chizhik, S. A.; Buzaneva, E. V.; Gorchinskiy, A. D. Layer-by-Layer Assembly of Ultrathin Composite Films from Micron-Sized Graphite Oxide Sheets and Polycations. *Chem. Mater.* **1999**, *11*, 771–778.

(34) Paredes, J. I.; Villar-Rodil, S.; Martinez-Alonso, A.; Tascon, J. M. D. Graphene oxide dispersions in organic solvents. *Langmuir* **2008**, *24*, 10560–10564.

(35) Hu, L.; Hecht, D. S.; Gruner, G. Percolation in Transparent and Conducting Carbon Nanotube Networks. *Nano Lett.* **2004**, *4*, 2513–2517.

(36) Kong, B. S.; Geng, J. X.; Jung, H. T. Layer-by-layer assembly of graphene and gold nanoparticles by vacuum filtration and spontaneous reduction of gold ions. *Chem. Commun.* **2009**, 2174–2176.

(37) Xu, Y. X.; Zhao, L.; Bai, H.; Hong, W. J.; Li, C.; Shi, G. Q. Chemically Converted Graphene Induced Molecular Flattening of 5,10,15,20-Tetrakis(1-methyl-4-pyridinio)porphyrin and Its Application for Optical Detection of Cadmium(II) Ions. *J. Am. Chem. Soc.* **2009**, *131*, 13490–13497.

(38) Casey, J. P.; Bachilo, S. M.; Weisman, R. B. Efficient photosensitized energy transfer and near-IR fluorescence from porphyrin-SWNT complexes. *J. Mater. Chem.* **2008**, *18*, 1510–1516.

(39) Guldi, D. M.; Rahman, G. M. A.; Jux, N.; Tagmatarchis, N.; Prato, M. Integrating single-wall carbon nanotubes into donor-acceptor nanohybrids. *Angew. Chem., Int. Ed.* **2004**, *43*, 5526–5530.

(40) Cioffi, C.; Campidelli, S.; Sooambar, C.; Marcaccio, M.; Marcolongo, G.; Meneghetti, M.; Paolucci, D.; Paolucci, F.; Ehli, C.; Rahman, G. M. A.; Sgobba, V.; Guldi, D. M.; Prato, M. Synthesis, characterization, and photoinduced electron transfer in functionalized single wall carbon nanohorns. *J. Am. Chem. Soc.* **2007**, *129*, 3938–3945.

(41) Szabo, T.; Berkesi, O.; Dekany, I. DRIFT study of deuterium-exchanged graphite oxide. *Carbon* **2005**, *43*, 3186–3189.

(42) Wu, Z. S.; Ren, W. C.; Gao, L. B.; Liu, B. L.; Jiang, C. B.; Cheng, H. M. Synthesis of high-quality graphene with a pre-determined number of layers. *Carbon* **2009**, *47*, 493–499.

(43) Stankovich, S.; Dikin, D. A.; Piner, R. D.; Kohlhaas, K. A.; Kleinhammes, A.; Jia, Y.; Wu, Y.; Nguyen, S. T.; Ruoff, R. S. Synthesis of graphene-based nanosheets via chemical reduction of exfoliated graphite oxide. *Carbon* **2007**, *45*, 1558–1565.

(44) Das, B.; Voggu, R.; Rout, C. S.; Rao, C. N. R. Changes in the electronic structure and properties of graphene induced by molecular charge-transfer. *Chem. Commun.* **2008**, 5155–5157.

(45) Das, A.; Pisana, S.; Chakraborty, B.; Piscanec, S.; Saha, S. K.; Waghmare, U. V.; Novoselov, K. S.; Krishnamurthy, H. R.; Geim, A. K.; Ferrari, A. C.; Sood, A. K. Monitoring dopants by Raman scattering in an electrochemically top-gated graphene transistor. *Nat. Nanotechnol.* **2008**, *3*, 210–215.

(46) McAllister, M. J.; Li, J.-L.; Adamson, D. H.; Schniepp, H. C.; Abdala, A. A.; Liu, J.; Herrera-Alonso, M.; Milius, D. L.; Car, R.; Prud'homme, R. K.; Aksay, I. A. Single Sheet Functionalized Graphene by Oxidation and Thermal Expansion of Graphite. *Chem. Mater.* **2007**, *19*, 4396–4404.

(47) Watcharotone, S.; Dikin, D. A.; Stankovich, S.; Piner, R.; Jung, I.; Dommett, G. H. B.; Evmenenko, G.; Wu, S.-E.; Chen, S.-F.; Liu, C.-P.; Nguyen, S. T.; Ruoff, R. S. Graphene-Silica Composite Thin Films as Transparent Conductors. *Nano Lett.* **2007**, *7*, 1888–1892.

(48) Wu, J. B.; Becerril, H. A.; Bao, Z. N.; Liu, Z. F.; Chen, Y. S.; Peumans, P. Organic solar cells with solution-processed graphene transparent electrodes. *Appl. Phys. Lett.* **2008**, *92*, 263302−1263302−3.

(49) Li, X. L.; Zhang, G. Y.; Bai, X. D.; Sun, X. M.; Wang, X. R.; Wang, E.; Dai, H. J. Highly conducting graphene sheets and Langmuir-Blodgett films. *Nat. Nanotechnol.* **2008**, *3*, 538–542.

JP1008779